RSC Advances

PAPER

View Article Online
View Journal | View Issue

Cite this: *RSC Adv.*, 2021, **11**, 7672

Synthesis of a DOTA-*C*-glyco bifunctional chelating agent and preliminary *in vitro* and *in vivo* study of [^{68}Ga]Ga-DOTA-*C*-glyco-RGD†

Floriane Mangin,[a] Charlotte Collet,[bc] Valérie Jouan-Hureaux,[d] Fatiha Maskali,[be] Emilie Roeder,[b] Julien Pierson,[d] Katalin Selmeczi,[a] Pierre-Yves Marie,[bef] Cédric Boura,[d] Nadia Pellegrini-Moïse *[a] and Sandrine Lamandé-Langle *[a]

The design of bifunctional chelating agents (BFCA) allowing straightforward radiometal labelling of biomolecules is a current challenge. We report herein the development of a bifunctional chelating agent based on a DOTA chelator linked to a *C*-glycosyl compound, taking advantage of the robustness and hydrophilicity of this type of carbohydrate derivative. This new BFCA was coupled with success by CuAAC with c(RGDfK) for $\alpha_v\beta_3$ integrin targeting. As attested by *in vitro* evaluation, the conjugate DOTA-*C*-glyco-c(RGDfC) demonstrated high affinity for $\alpha_v\beta_3$ integrins (IC_{50} of 42 nM). [^{68}Ga]Ga-DOTA-*C*-glyco-c(RGDfK) was radiosynthesized straightforwardly and showed high hydrophilic property (log $D_{7.4}$ = −3.71) and *in vitro* stability (>120 min). Preliminary *in vivo* PET study of U87MG engrafted mice gave evidence of an interesting tumor-to-non-target area ratio. All these data indicate that [^{68}Ga]Ga-DOTA-*C*-glyco-c(RGDfK) allows monitoring of $\alpha_v\beta_3$ expression and could thus be used for cancer diagnosis. The DOTA-*C*-glycoside BFCA reported here could also be used with various ligands and chelating other (radio)metals opening a broad scope of applications in imaging modalities and therapy.

Received 31st October 2020
Accepted 9th February 2021

DOI: 10.1039/d0ra09274f

rsc.li/rsc-advances

Introduction

Peptides are an important class of ligands and have emerged in molecular imaging and nuclear medicine due to their advantageous properties, which include high target specificity and selectivity, low toxicity, biocompatibility and biodegradability.[1–3] In particular, radiolabelled peptides or proteins are suitable for positron emission tomography (PET)[1,4–8] as new diagnostic agents for preclinical and clinical research and are today considered as fully "druggable" moieties.[2]

Peptides can be radiolabelled with fluorine-18 (^{18}F) by addition of a fluorinated prosthetic group or with radiometals (gallium-68, copper-64 or zirconium-89) through a bifunctional chelating agent (BFCA).[1,9,10] However, this structural modification can disrupt the metabolic profile and/or decrease the affinity of the biomolecule for its biological target, which is a major drawback, in particular for molecular imaging. In light of this, it is worth noting that the introduction of a carbohydrate moiety on biomolecules, such as peptides, has often been shown to enhance their pharmacokinetic and *in vivo* clearance properties.[5,11–13]

^{18}F-glycopeptides, obtained by attachment of a radiofluorinated carbohydrate entity on peptides for an application in PET imaging have been a subject of interest in our group for several years. In particular, RGD peptide derivatives are selective for $\alpha_v\beta_3$ integrins, which are important cell adhesion receptors involved in angiogenic processes allowing cancer diagnosis.[4,14,15] Various ^{18}F-glyco-RGD containing an *O*- or a *C*-glycosidic moiety conjugated with a RGD peptide derivative have been designed, synthetized and their automated radiosynthesis has been developed.[4,5,16,17] However, ^{18}F-radiolabelling of biomolecules remains a challenge because it requires time consuming multistep automated radiosyntheses.

The use of radiometals allows straightforward peptides radiolabelling by simple metal coordination *via* a chelating agent previously introduced on the peptide. Furthermore, ^{68}Ga-labelled peptides are attracting increasing interest in PET diagnostics because ^{68}Ga is easily produced with a [^{68}Ge]/[^{68}Ga] generator thus not requiring a biomedical cyclotron, and its short half-life of 68 min reduces the radiation burden to the patient.

DOTA (1,4,7,10-tetraazacyclododecane-1,4,7,10-tetraacetic acid) is one of the most important chelator in the field of medical imaging and molecular radiotherapy.[1,18–20] Undoubtedly, this azamacrocycle forms very stable complexes with

[a]*Université de Lorraine, CNRS, L2CM, F-5400 Nancy, France. E-mail: Sandrine.langle@univ-lorraine.fr; Nadia.pellegrini@univ-lorraine.fr*
[b]*NancycloTEP, Molecular Imaging Platform, CHRU-Nancy, Université de Lorraine, Nancy, F-54000, France*
[c]*Université de Lorraine, INSERM, U1254 IADI, F-54000 Nancy, France*
[d]*Université de Lorraine, CNRS, CRAN, F-54000 Nancy, France*
[e]*Université de Lorraine, INSERM, DCAC, UMR 1116, F-54000 Nancy, France*
[f]*Department of Nuclear Medicine, CHRU-Nancy, F-54000 Nancy, France*

† Electronic supplementary information (ESI) available: Experimental details and physico-chemical characterization of new compounds and quality control protocols. See DOI: 10.1039/d0ra09274f

a variety of metal ions, such as lanthanides and radionuclides, explaining its wide range of applications in the main imaging modalities *i.e.* Magnetic Resonance (MRI), Single Photon Emission Computed Tomography (SPECT) and Positron Emission Tomography (PET), and also for therapeutic purposes.[21–26] This prompted research into the chemistry of DOTA, in particular on the modification of the side arm of the azamacrocycle.[27,28] For example, the side arm has been derivatized with different polyethylene glycol moieties (PEG), amino acids or aliphatic chains displaying functional group like amine, carboxylic acid or azide for subsequent coupling with targeting molecules.[27,29–31]

In close link with our interests in PET radiotracers, we have designed an original strategy for ^{68}Ga-labelling of peptides and we have implemented this method for the preparation of ^{68}Ga-labelled glyco-RGD. A new bifunctional chelating agent named DOTA-*C*-glyco was elaborated by linking the common polyazamacrocycle DOTA and a functional carbohydrate moiety. This latter bears an azido-arm which enables the conjugation of biological vectors of interest, by Copper-catalyzed Azide-Alkyne Cycloaddition (CuAAC) with a propargylated peptide such as propargylated c(RGDfK). The ability of the synthesized DOTA-*C*-glyco-c(RGDfK) to target integrins was evaluated *in vitro* by a solid-phase binding assay. ^{68}Ga-labelling was carried out and PET imaging was implemented to assess the performance of this new ^{68}Ga-labelled radiotracer for cancer diagnosis.

Results

Chemistry

The construction of DOTA-*C*-glycopeptide requires the preliminary synthesis of the DOTA-*C*-glyco bifunctional chelating agent. We first investigated the preparation of a DOTA moiety bearing an amino functional arm for the conjugation with the *C*-glycoside. To this end, *N*-(2-benzyloxycarbonylaminoethyl)bromoacetamide **1** was chosen (Scheme 1).[32] The commercially available protected tri-*tert*-butyl-1,4,7,10-tetraazacyclododecane-1,4,7-triacetate (DO3A(*t*-BuO)) **2** was *N*-alkylated with **1** using K_2CO_3 and few drops of dimethylformamide in dry acetonitrile. The removal of the Cbz protecting group by catalytic hydrogenolysis was carried out under H_2 (atmospheric pressure) with Pd/C-10% (10% w/w) in methanol to furnish compound **4** in quantitative yield.[32]

The synthesis of the glycosidic derivative was then carried out taking advantage of our precedent work on the synthesis of fluoro-*C*-glyco-RGD.[4] Interestingly, the robust C–C link at the anomeric position displays a high resistance to acidic and enzymatic hydrolysis, conferring an improved *in vivo* stability to *C*-glycosyl compounds compared to *O*-glycosides.[4,33] A *C*-glycoside moiety with a 3-carbon spacer-arm bearing an azido group for the CuAAC reaction was thus investigated. The pseudo-anomeric position was chosen for the azido propyl arm introduction given the high reactivity of this position. A protection/deprotection strategy allowed us to generate a reactive primary hydroxyl group and its tosylated counterpart in position 6 (sugar numbering) for DOTA coupling. Azido-*C*-glyco derivative **7** was synthesized as previously described (Scheme 2).[4] Briefly, 1-*O*-acetyl-2,3,4,6-tetra-*O*-benzyl-D-glucopyranose **5** was stereoselectively converted with allyl bromide into β-*C*-allylglucopyranoside subsequently treated with 9-borabicyclo(3.3.1)nonane (9-BBN) to furnish the resulting alcohol. The latter was then converted to bromide derivative **6** *via* a bromination reaction followed by hydrogenolysis of the benzyl ether protecting groups under H_2 atmosphere. Compound **6** was reacted with sodium azide, underwent a selective tritylation of the primary alcohol, then peracetylation and trityl group removal provided compound **7**.[4] Lastly, tosylated compound **8** was obtained in 52% yield after reaction of **7** with tosyl chloride, triethylamine and a catalytic amount of dimethylaminopyridine (DMAP).

Having in hand DOTA derivative **4** and *C*-glycoside compounds **7** and **8**, their coupling was examined. We first attempted a *N*-alkylation of **4** with tosylated compound **8**. Unfortunately, the reaction did not occur and the starting materials were recovered even after modification of various parameters such as the nature of the solvent (acetonitrile or DMF), temperature (30 or 80 °C), reaction time and stoichiometry. A second strategy based on the formation of a carbamate bond has been explored (Scheme 3). Reaction of **7** with *N*,*N*-carbonyldiimidazol (CDI) was performed in dioxane to give intermediate **9** (62%). The imidazolylcarbonyl derivative **9** was treated with compound **4** in the presence of triethylamine to afford the protected DOTA-glycoconjugate **10** in 53% yield. Deprotection of *tert*-butyl ester and acetyl protecting groups with an aqueous solution of 4N HCl at room temperature during 4 hours led to compound **11** quantitatively.

The introduction of the peptide on DOTA-*C*-glyco tool **11** was performed site-specifically by CuAAC with alkyne-modified c(RGDfK) **12**.[34] The reaction proceeded efficiently under very

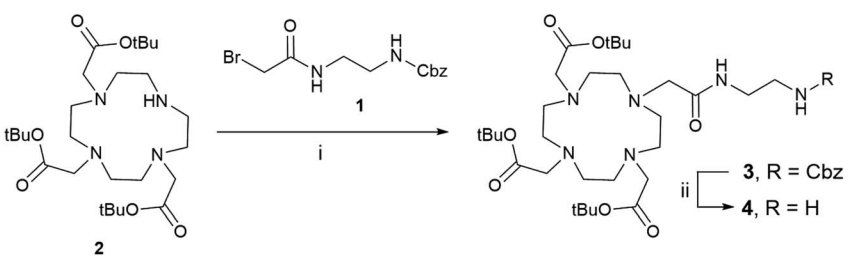

Scheme 1 DOTA derivative synthesis. Reagents and conditions: (i) K_2CO_3, DMF, dry acetonitrile, rt, 12 h, 52%; (ii) H_2, Pd/C-10% (10% w/w), MeOH, rt, 5 h, quantitative.

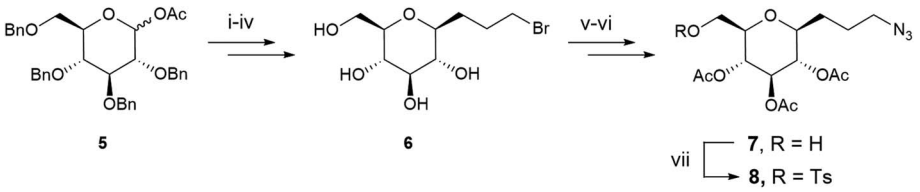

Scheme 2 *C*-glycoside derivative synthesis. Reagents and conditions: (i) TMSI, CH_2Cl_2, 0 °C, 1 h, then AllylMgBr, 0 °C to rt, 3 h, 90%; (ii) (1) 9-BBN, THF, Δ, 4 h; (2) EtOH, NaOH, H_2O_2, 12 h, 89%; (iii) PPh_3, CBr_4, CH_2Cl_2, 0 °C, 1 h, 90%; (iv) $Pd(OH)_2$/C (20% w/w), THF/H_2O (5/1 v/v), H_2, 33 psi, 13 h, 93%; (v) NaN_3, acetone/water (5/1 v/v), reflux, 12 h, 95%; (vi) (1) TrCl, DMAP, pyridine, 48 h, 45 °C. (2) Ac_2O, 0 °C to rt, 2 h, 62%; (vi) TFA (20% v) in CH_2Cl_2, 0 °C, 10 min, 73%; (vii) tosyl chloride, DMAP cat., triethylamine, CH_2Cl_2, 12 h, 30 °C, 52%.

mild conditions in a water/*tert*-butanol solution (1/1 v/v) using copper(II) acetate (1.5 equivalents) and sodium ascorbate (3 equivalents) as reducing agent (Scheme 3). A stoichiometric quantity of copper(II) acetate was required instead of the catalytic amounts usually employed, because copper ions were chelated by the DOTA macrocycle. Furthermore, the removal of complexed Cu^{2+} from the cage proved tricky. Indeed, the classical strategy using a chelating resin (Chelex®) has failed. In our case, the best solution was the addition of 6 equivalents of sodium sulfide nonahydrate leading to the precipitation of copper(II) as monosulfide.[35] After filtration on a Celite pad and freeze-drying, purification by steric exclusion gel filtration was performed affording DOTA-*C*-glyco-c(RGDfK) **13** in a high yield of 72%. High resolution mass spectrometry as well as 1D and 2D NMR data confirmed the structure of the conjugate.

The gallium(III) complex of compound **13**, **(Ga)13**, was also synthetized in order to evaluate its *in vitro* affinity for $\alpha_v\beta_3$ integrin. For the complexation reaction, 1 equivalent of gallium(III) nitrate was added to a solution of compound **13** in water and the mixture was heated for 20 min at 110 °C. After freeze-drying, Ga-DOTA-*C*-glyco-c(RGDfK) **(Ga)13** was obtained as a white powder. The gallium(III) ion complexation was confirmed by mass spectrometry, the measured *m*/*z* values and the observed isotopic patterns are in good agreement with those calculated for $C_{60}H_{93}N_{18}O_{21}Ga$ $[M + Ga]^{2+}$ (calcd. 735.3006, found 735.3004) and for $C_{60}H_{93}N_{18}O_{21}GaNa$ [M + Ga + Na]3+ (calcd. 497.8637, found 497.8633) (see ESI†).

Integrin $\alpha_v\beta_3$ binding assay

The affinity of compounds **13** and **(Ga)13** for $\alpha_v\beta_3$ integrin was evaluated by a solid-phase binding assay (Fig. 1). The results showed that the IC_{50} values of **13** and **(Ga)13** (77 and 45 nM respectively), although slightly lower than the reference positive controls Echistatin (4 nM) and c(RGDfK) (16 nM), remain in the nanomolar range. These data demonstrate a high affinity of **13** and **(Ga)13** for the $\alpha_v\beta_3$ integrin.

Radiochemistry

DOTA-*C*-glyco-c(RGDfK) **13** was radiolabelled with gallium-68 on a MiniAllInOne (Trasis®) synthesiser (Scheme 4). Different parameters such as amount of **13**, reaction time and temperature were screened. The optimal amount of compound **13** was found to be 50 μg in 1 mL of 0.7 M acetate solution (pH = 7.9). As commonly described for ^{68}Ga-DOTA radiolabelling, a temperature of 110 °C was required to reach maximum gallium-68 chelation for a reaction time of 10 min (86% determined by HPLC analyses). Formulation of the resulting [^{68}Ga]

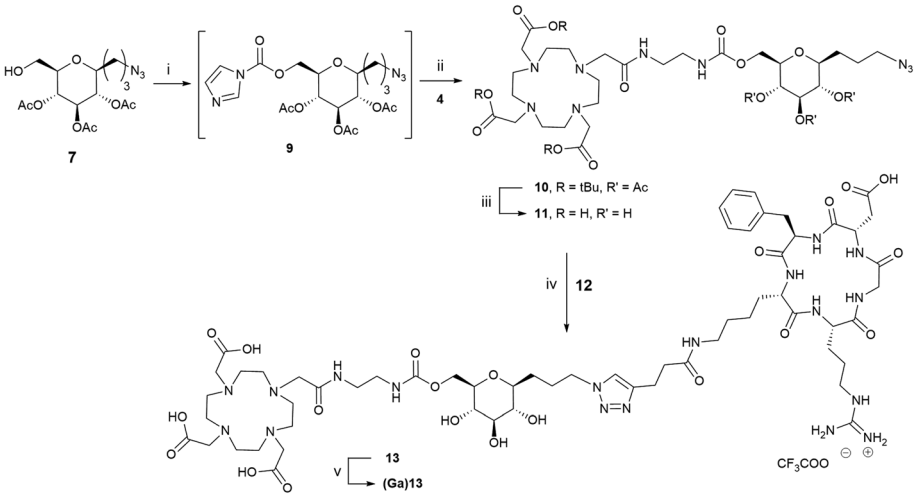

Scheme 3 DOTA-*C*-glyco and DOTA-*C*-glyco-c(RGDfK) synthesis. Reagents and conditions: (i) *N*,*N*-carbonyldiimidazole, dioxane, rt, 62%. (ii) **4**, triethylamine, dry THF, rt, 12 h, 53%. (iii) H_2O, 4N HCl, rt, 4 h, quantitative. (iv) (1) H_2O/*tert*-butanol 1/1 v/v, sodium ascorbate, $Cu(OAc)_2$, rt, 5 h. (2) $Na_2S{\cdot}9H_2O$, rt, 15 min, 72%. (v) $Ga(NO_3)_3$, H_2O, 110 °C, 20 min.

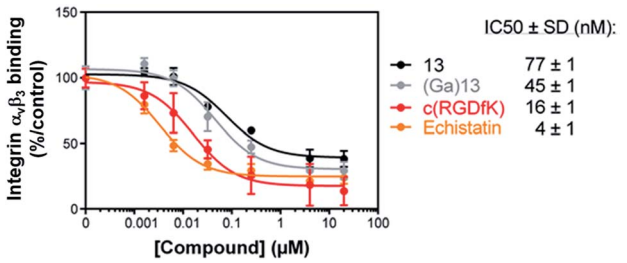

Fig. 1 Solid-phase binding assay. Effect of **13** (dark) and **(Ga)13** (grey) on the binding of $\alpha_v\beta_3$ integrin onto vitronectin compared with two reference molecules: c(RGDfK) (red) and Echistatin (orange). IC_{50} values (nM) were calculated using one-site fit log-IC_{50} non-linear analysis regression (graphpad prism).

Ga-DOTA-*C*-glyco-c(RGDfK) was performed on a HLB Oasis cartridge, eluted with 0.6 mL of ethanol and washed with 4.5 mL of 0.9% NaCl. [^{68}Ga]Ga-DOTA-*C*-glyco-c(RGDfK) was straightforwardly radiosynthesised in 78 ± 3% ($n = 20$) decay corrected radiochemical yield. Typical preparation run produced in average 175 MBq of 5 mL of **[^{68}Ga]13** solution in approximately 30 minutes starting from activity elution.

Quality control of radiotracer **[^{68}Ga]13** was carried out on an aliquot of the final batch. The radiotracer solution was clear and colorless with a pH around 5.5–6. Radiochemical and chemical purities were evaluated by analytical HPLC on a C_{18} column using UV and radioactive detection. UV chromatogram showed no by-products demonstrating high chemical purity. The radiochemical purity was determined to be over 95% with a molar activity average of 5 MBq per nmol. *In vitro* plasma stability of **[^{68}Ga]13** was also determined at 37 °C in rodent plasma by radioactive HPLC detection. Analyses of acetonitrile plasma extracts at selected time points (0, 30, 60 and 120 min) demonstrated an *in vitro* stability >120 min for compound **[^{68}Ga]13.** Experimental log $D_{7.4}$ of −3.71 (*n*-octanol/PBS pH 7.4 partition coefficient) showed excellent hydrophilic property for **[^{68}Ga]13.**

PET imaging

A series of dynamic images (coronal sections) were obtained up to 120 min after the injection of **[^{68}Ga]13** on whole-body PET images of U87MG engrafted mice (Fig. 2a). $\alpha_v\beta_3$ integrins, which are targeted by RGD-containing tracers, are highly expressed in high-grade gliomas in which the magnitude of this expression has been associated with the potential for tumor invasion, angiogenesis, and metastasis.[36,37]

Corresponding time–activity curves for tumor and non-target area (contralateral area) showed that the uptake of **[^{68}Ga]13** increased faster in the tumor than in the non-target area (Fig. 2b), resulting in an enhancement of the tumor-to-non-target area ratio during 120 min of dynamic analysis (Fig. 2c). Otherwise, **[^{68}Ga]13**, showed a fast renal clearance resulting in particularly high activities in the kidneys and bladder.

Whole-body image of the second hour of PET recordings is depicted in Fig. 3a, providing an illustration of the potential of **[^{68}Ga]13** for tumor imaging. The Fig. 3b shows the mean standard value uptakes within various organs of reference (heart, brain, kidney, liver), within the tumor and within a non-target area (contralateral area). The Fig. 3c displays the uptake ratios of the tumor *versus* the area cited above. These data were computed for the second hour of PET recording and showed the radiotracer profile. High radioactivity accumulation was observed in the kidneys, showing a raised clearance of the tracer during the second hour. Moreover, the tumor activity from **[^{68}Ga]13**, which likely corresponds to integrin binding, was found two-fold higher than that of the non-target region (0.21 ± 0.04 *vs.* 0.10 ± 0.01; $p < 0.05$ for SUVmean of tumor and non-target area respectively), and approximatively four times higher than that of normal brain (0.06 ± 0.01), giving high tumor-to-non-target area (2.20 ± 0.45) and tumor-to-brain (3.90 ± 0.10) ratios.

Discussion

The development of new diagnostic/therapeutic tools for molecular imaging like PET or molecular radiotherapy, combining high affinity toward receptor, high *in vivo* stability and optimal pharmaco-kinetic profile remains a daunting challenge. Bioavailability is another crucial characteristic, especially in the context of PET imaging relying on radioisotopes with short half-lives. In this paper, we have designed an original DOTA-*C*-glyco-c(RGDfK) containing a *C*-glycosyl moiety bearing an azido spacer-arm. Having a stable and non-hydrolysable C–C link at the pseudo-anomeric position, *C*-glycosyl compounds are key components for the construction of

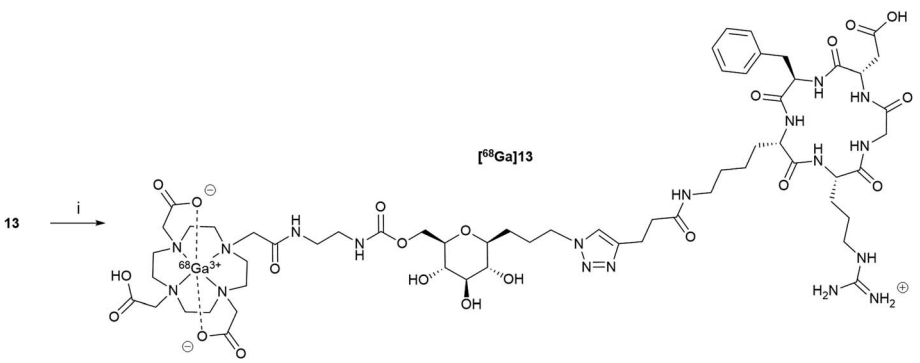

Scheme 4 Radiosynthesis of **[^{68}Ga]13**. Reagents and conditions: (i) [^{68}Ga]$GaCl_3$, AcONa (0.7 M) 110 °C, 10 min, 78 ± 3% dc.

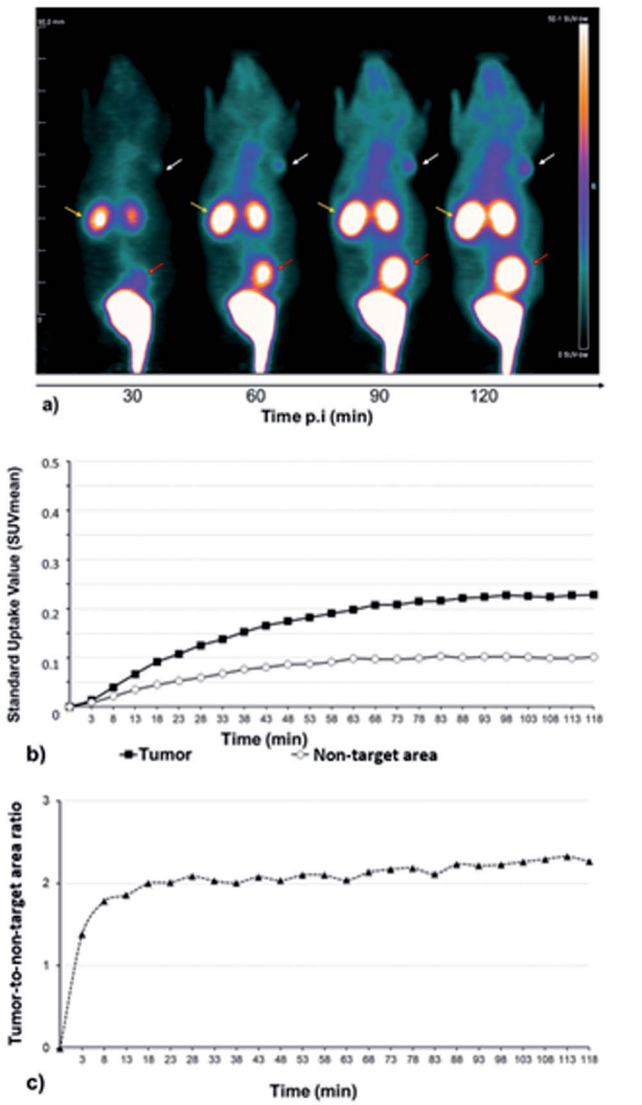

Fig. 2 (a) Dynamic PET images displayed through coronal sections and recorded during 120 min following [^{68}Ga]**13** injection in U87MG engrafted mice (n = 3). Color scale is expressed in SUV values. The tumors are indicated with white arrows, the kidneys with yellow arrows and the bladder with red arrows. (b) Corresponding time–activity curves for mean SUV from tumor (black square) and from non-target area (white circle), as well as for tumor-to-non-target area ratio (black triangles) (c).

stable glycoconjugates for various *in vivo* applications.[4,33,38] Besides, the DOTA-*C*-glycoside tool bears an azide group to ensure CuAAC conjugation with biological ligands. This strategy allows a site-specific conjugation to a large panel of ligands previously derivatized with an alkyne function. Previous works on *C*-glyco-RGD derivatives showed adequate flexibility and ideal steric arrangement with a three-carbon spacer-arm, conferring them similar affinities toward $\alpha_v\beta_3$ integrin than the native RGD.[4] Given the importance of maintaining the highest affinity, an analogous *C*-glycosyl compound was chosen for the design of the tracer. We conjugated with success the DOTA-*C*-glycosyl derivative on alkyne-modified c(RGDfK) peptide for $\alpha_v\beta_3$ integrin targeting. Compared to common DOTA-c(RGDfK),[39,40] the *C*-glycosyl moiety with a long spacer arm afforded a distance between DOTA and the peptide, which is obviously favourable for binding. The gallium(III) complexed counterpart of this DOTA-glycopeptide was also successfully synthesized.

In vitro evaluation and comparison of derivative DOTA-*C*-glyco-c(RGDfK) **13** were carried out with the gold standard integrin inhibitor Echistatin and with native c(RGDfK). To be as close as possible to the ^{68}Ga-radiolabelled form injected for PET imaging, Ga-DOTA-*C*-glyco-c(RGDfK) **(Ga)13** was also evaluated in the same experimental protocol. In many cases, the addition of reporting moieties like fluorophores or chelating agents affects the binding affinity of the modified biomolecules. In our case, compounds **(Ga)13** and **13** presented a slight decrease of affinity compared to Echistatin and native RGD, however, remaining in the same nanomolar range. These data showed that the Ga-DOTA complex and the carbohydrate linker did not significantly impede the affinity of c(RGDfK) peptide for $\alpha_v\beta_3$ integrin. The binding affinity of **(Ga)13** is slightly greater compared to compound **13**. However, both IC_{50} are in the same range (42 nM *vs.* 75 nM for **(Ga)13** and **13** respectively).

[^{68}Ga]**13** was synthesized straightforwardly in high radiochemical yields and purity. Incorporation of gallium-68 into the DOTA requires heating to 110 °C, however, despite this weakness, this chelator was chosen for its versatility towards other metal ions. Some other chelator like the acyclic HBED-CC or the NOTA require lower energy for complex formation. However, HBED-CC forms different diastereomers upon complexation of gallium, which is undesirable because different isomers may have different pharmacological profiles. Whereas NOTA does not present the optimal number of coordination site for the chelation of other metals used in medical imaging and molecular radiotherapy.[41,42] Experimental partition coefficient (−3.71) demonstrated excellent hydrophilic property for [^{68}Ga]**13**. This value is slightly lower than those of commonly used [^{68}Ga]Ga-DOTA-c(RGDfK) (around −3.43)[40] indicating an improved hydrophilicity which could be attributed to the carbohydrate moiety.

A 120 min dynamic PET imaging with [^{68}Ga]**13** showed a slow increasing uptake of the tracer in the tumor and non-target area up to 60 min post injection of [^{68}Ga]**13**. This observation is in accordance with previous literature on RGD-containing tracers, leading to the current recommendation of delaying PET recording for 30 to 60 min after tracer injection.[43–46] This avoids an early high level of nonspecific activity, possibly due to the circulating blood tracers, and thus prevents overestimation of integrin density. The 120 min time activity curves of biodistribution of [^{68}Ga]**13** showed a higher uptake of the tracer in the tumor than in the non-target area, suggesting a specific uptake of [^{68}Ga]**13** by $\alpha_v\beta_3$ integrin in glioblastoma. These integrins, highly expressed in high-grade gliomas, are known to be poorly expressed within the different tissue components of normal brain. These considerations likely explain the high tumor-to-normal brain ratio documented herein for [^{68}Ga]**13**, *i.e.*, 3.90 ± 0.10 for this mouse model. These data combined with high *in vitro* stability and affinity toward $\alpha_v\beta_3$ integrin makes [^{68}Ga]**13** a potential radiotracer for cancer diagnosis.

The synthesized DOTA-*C*-glycosyl bifunctional chelating agent is a versatile tool. In this study, it has been studied and

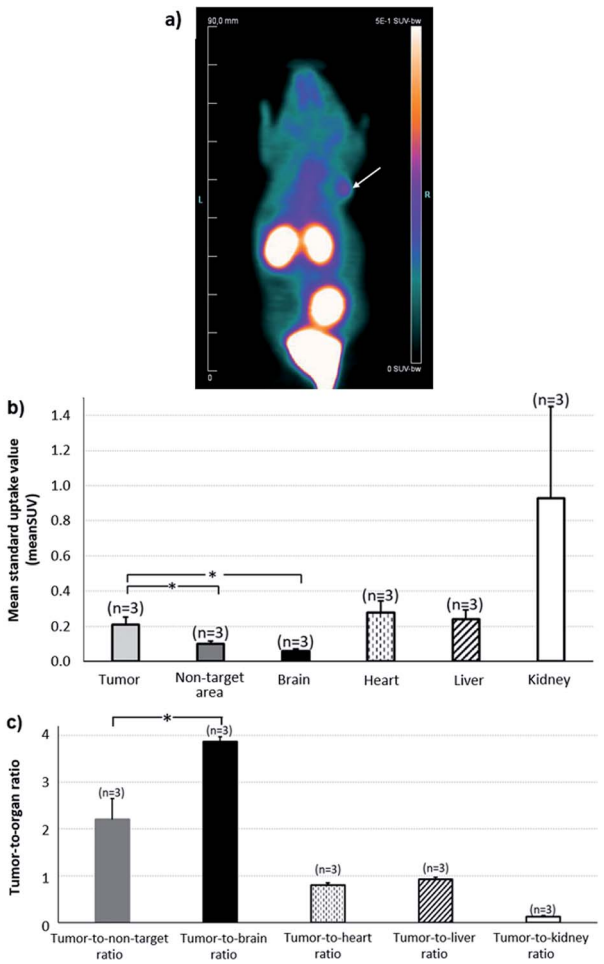

Fig. 3 (a) Whole-body image of the 2nd hour of PET recordings after [^{68}Ga]**13** injection. (b) Results of SUVmean values obtained at the 2nd hour of PET recording for tumors and various organs, after the injection of [^{68}Ga]**13**. (c) Comparison of tumor-to-organ ratio for activities measured during the 2nd hour of PET recording. *: $p < 0.05$ The tumor is indicated with white arrows and the color scale is expressed in SUV values ($n = 3$).

illustrated with gallium-68 labelling of an RGD peptide derivative, however this BFCA could be used with others biological ligands like peptides, proteins or antibodies and for other medical applications. Indeed, DOTA is widely used in the field of medical imaging and molecular radiotherapy because it chelates efficiently a large panel of (radio)metals. Hydrophilic BFCA **11** could be potentially suitable for different imaging modalities and therapy, such as PET (^{68}Ga, ^{64}Cu), SPECT (^{99m}Tc, ^{111}In) and MRI (Gd). Besides, targeted cancer therapy might also be possible with DOTA-*C*-glycoside **11** labelled with ^{177}Lu, ^{90}Y or ^{186}Re. DOTA-*C*-glyco could also be employed in theranostics enabling concomitant diagnostic and radiotherapy by labelling with diagnostic and therapeutic radioisotopes.

Conclusion

In this study, we reported for the first time the synthesis of DOTA-*C*-glycosyl bifunctional chelating agent (BFCA) and its conjugation to c(RGDfK) peptide using CuAAC. The design of the DOTA-*C*-glyco BFCA exploited the hydrophilicity and the robustness of *C*-glycosyl moiety. *In vitro* binding of DOTA-*C*-glyco-c(RGDfK) and its gallium(III) complexed counterpart, to $\alpha_v\beta_3$ integrin showed that conjugation of DOTA-*C*-glycoside to c(RGDfK) did not affect its affinity. [^{68}Ga]Ga-DOTA-*C*-glyco-c(RGDfK) **[^{68}Ga]13** was radiosynthesized straightforwardly and showed high hydrophilic property ($\log D_{7.4} = -3.71$) and *in vitro* stability (>120 min). Tumor-to-non-target area ratio obtained by *in vivo* PET study in U87MG engrafted mice, demonstrated that [^{68}Ga]Ga-DOTA-*C*-glyco-c(RGDfK) could be a potential radiotracer for cancer diagnosis by PET imaging. As reported in this study, the DOTA-*C*-glycoside BFCA is a versatile tool, successfully employed for ^{68}Ga-radiolabelling of c(RGDfK). Furthermore, the possibility of using others ligands and (radio)metals opens a broad scope of applications in imaging modalities and therapy.

Experimental section

General information

Solvents and liquid reagents were purified and dried according to recommended procedures. Thin layer chromatography (TLC) analyses were performed using standard procedures on Kieselgel 60F254 plates (Merck, Kenilworth, NJ, USA). Compounds were visualized using UV light (254 nm), ninhydrin and/or a methanolic solution of sulfuric acid and charred. Column chromatography was performed on silica gel SI 60 (63–200 μm) (Merck). c(RGDfK) was purchased from Bachem (Germany) with >95% purity. Purification of RGD-conjugate was achieved by gel filtration on LH20 using water as eluent. Melting points were determined with a Tottoli apparatus and are uncorrected. FTIR spectra were recorded on a Shimadzu IRAffinity-1, ATR PIKE Technologies model GladiAT (cm^{-1}). Optical rotations were measured on an Anton-Paar MCP 300 polarimeter. Analytical High Performance Liquid Chromatography (HPLC) analyses were run on a Waters system (2695eb pump, auto sampler injector, 2998 PDA detector, 2424 ELSD detector, and NaI detector from Berthold [Bad Wildbad, Germany]) controlled by the Empower Software (Orlando, FL, USA). Analyses were performed on a Vydac 218 TP C18 (5 μm, 250 × 4.6 mm) from Grace with ACN/H_2O/TFA mixture (proportions given in brackets) at 1 mL min^{-1}. ^{1}H, ^{13}C, and ^{19}F NMR spectra were recorded on a Bruker DPX250 (250 MHz, 62.9 MHz and 235 MHz, respectively) or DRX400 (400 MHz and 100.6 MHz, respectively) spectrometers on the NMR Platform of the Jean Barriol Institute (Université de Lorraine, Nancy, France). For complete assignment of ^{1}H and ^{13}C signals, two-dimensional ^{1}H, ^{1}H COSY and ^{1}H, ^{13}C correlation spectra were recorded. Chemical shifts (δ) are given in parts per million relative to the solvent residual peak. For clarity, atom numbering starts from the end of the anomeric arm rather than resulting from the IUPAC naming of compounds (see ESI Fig S1†). The following abbreviations are used for multiplicity of NMR signals: s = singlet, d = doublet, t = triplet, q = quadruplet, m = multiplet, b = broad signal and app = apparent multiplicity. The given *J* values refer to apparent multiplicities and do not represent the true coupling constants. High resolution ESI-MS spectra were recorded on a Bruker

Daltonics microTOFQ apparatus provided by the MassLor Platform (Université de Lorraine, Nancy, France). $^{68}GaCl_3$ was eluted from a $^{68}Ge/^{68}Ga$ generator (Galliapharm; Eckert & Ziegler Europe) with 5 mL of a 0.1 N HCl solution. Radiosynthesis was carried out on a miniAllInOne (miniAIO) module from Trasis®. Female immunodeficient (nu/nu) NMRI mice were purchased from Janvier Laboratories. PET recordings were obtained with a camera dedicated to small animal studies (Inveon, Siemens Preclinical Solutions, Knoxville, USA).

Experimental procedures and physico-chemical characterizations

Chemistry. Compounds **1**,[32] **2**,[32] **4**,[32] **6**,[4] **7** (ref. 4) and **12** (ref. 34) were prepared according to previously described methods (see ESI†).

*4,8-Anhydro-1-azido-1,2,3-trideoxy-5,6,7-tri-O-acetyl-9-O-tosyl-D-glycero-D-gulo-nonitol (**8**).* To a solution of 4,8-anhydro-1-azido-1,2,3-tridesoxy-5,6,7-tri-*O*-acetyl-D-*glycero*-D-gulo-nonitol (424 mg, 1.14 mmol) in dry DCM (10 mL) tosyl chloride (658.4 mg, 3.42 mmol), DMAP (66 mg, 0.57 mmol) and triethylamine (0.63 mL, 4.54 mmol) were added under argon. The reaction was stirred overnight at 30 °C. The mixture was concentrated under reduced pressure and purified on by flash column chromatography (silica gel, Cyclohexane/EtOAc 6/4) to afford **8** (607 mg). Yield 52%. White solid. Mp: 78–80 °C; $[\alpha]_D$: +12.0 (c 0.09; EtOH); IR film (ν, cm^{-1}): 2102, 1738, 1599, 1368, 1256, 1227, 1188, 1173, 1119, 1098, 1032; ^1H NMR (400 MHz, $CDCl_3$): δ 1.36–1.46 (m, 1H, H3a), 1.51–1.63 (m, 2H, H2a and H3b), 1.68–1.78 (m, 1H, H2b), 1.98 (s, 3H, CH_3), 1.99 (s, 3H, CH_3), 2.03 (s, 3H, CH_3), 2.46 (s, 3H, CH_3), 3.20–3.31 (m, 2H, $J_{1,2a} = J_{1,2b} = 6.5$ Hz, H1), 3.38 (bddd, 1H, $J_{4,5} = 9.5$ Hz, $J_{4,3b} = 9.0$ Hz, $J_{4,3a} = 2.5$ Hz, H4), 3.66 (ddd, 1H, $J_{8,7} = 9.0$ Hz, $J_{8,9b} = 6.0$ Hz, $J_{8,9a} = 3.0$ Hz, H8), 4.02 (dd, 1H, $J_{9a,9b} = 11.0$ Hz, H9a), 4.09 (dd, 1H, H9b), 4.80 (app t, 1H, $J_{4,5} = J_{5,6} = 9.5$ Hz, H5), 4.89 (app t, 1H, $J_{7,6} = J_{8,7} = 9.0$ Hz, H7), 5.13 (app t, 1H, H6), 7.35 (d, 2H, $J = 8.0$ Hz, Ar), 7.78 (d, 2H, $J = 8.0$ Hz, Ar). ^{13}C NMR (100.6 MHz, $CDCl_3$): δ 20.7 (CH_3), 20.7 (CH_3), 20.8 (CH_3), 21.8 (CH_3), 24.6 (C2), 28.4 (C3), 51.2 (C1), 68.1 (C9), 69.0 (C7), 71.7 (C5), 74.1 (C6), 75.5 (C8), 77.4 (C4), 128.2 ($2C_{Ar}$), 130.0 ($2C_{Ar}$), 132.7 (C_q), 145.3 (C_q), 169.6 (C═O), 169.7 (C═O), 170.4 (C═O). HRMS (ESI, $C_{22}H_{29}N_3O_{10}SNa$: $[M + Na]^+$) calcd 550.1471, found 550.1493.

*Compound **10**.* To a solution of 4,8-anhydro-1-azido-1,2,3-trideoxy-5,6,7-tri-*O*-acetyl-D-*glycero*-D-gulo-nonitol **7** (75 mg, 0.2 mmol) in dioxane (1.4 mL), was added under argon, *N*,*N*-carbonyldiimidazole (38.9 mg, 0.24 mmol). The mixture was stirred at room temperature until completion of the reaction (TLC monitoring), then was concentrated under reduced pressure. The residue was diluted in a cyclohexane/EtOAc 1/1 v/v solution (5 mL), filtered on a silica gel pad and evaporated under reduced pressure to obtain intermediate **9** as a colorless oil (57.8 mg, 62%). To a solution of **9** in dry THF (2 mL), **4** (110.8 mg, 0.18 mmol) and triethylamine (167 μL, 1.2 mmol) were added. The reaction mixture was stirred overnight at room temperature. After evaporation under reduced pressure, the crude product was purified by LH20 chromatography with MeOH as eluant, then by flash chromatography (silica, CH_2Cl_2/MeOH 9/1) to afford compound **10** (64.5 mg). Yield 53%. Yellow solid. Mp: 99–101 °C; $[\alpha]_D$: + 3.6 (c 0.05; EtOH); IR film (ν, cm^{-1}): 2976, 2816, 2093, 1722, 1668, 1520, 1368, 1221, 1155, 1105, 1030. ^1H NMR (400 MHz, DMSO-d6): δ 1.36–1.43 (m, 1H, H3a), 1.45 (s, 18H, *t*Bu), 1.46 (s, 9H, *t*Bu), 1.54–1.64 (m, 2H, H2), 1.65–1.74 (m, 1H, H3b), 1.93 (s, 3H, CH_3), 1.98 (s, 3H, CH_3), 2.00 (s, 3H, CH_3), 2.24–2.41 (m, 8H, CH_2 cyclen), 2.54–2.70 (m, 8H, CH_2 cyclen), 3.00–3.21 (m, 12H, H11, H12, H14, H17, H20, H23), 3.33 (t, 2H, $J_{1,2a} = J_{1,2b} = 6.5$ Hz, H1), 3.64 (b ddd, 1H, $J_{8,7} = 10.0$ Hz, $J_{8,9b} = 7.5$ Hz, $J_{8,9a} = 2.5$ Hz, H4), 3.80 (b ddd, 1H, $J_{8,7} = 8.0$ Hz, $J_{8,9b} = 5.0$ Hz, $J_{8,9a} = 3.0$ Hz, H8), 4.02 (dd, 1H, $J_{9a,9b} = 12.0$ Hz, $J_{9a,8} = 3.0$ Hz, H9a), 4.07 (dd, 1H, $J_{9b,8} = 5.0$ Hz, H9b), 4.71 (app t, 1H, $J_{7,6} = 9.5$ Hz, H5), 4.88 (dd, 1H, $J_{5,6} = 9.5$ Hz, H7), 5.17 (app t, 1H, H6), 6.87 (bs, 1H, NH), 7.93 (bs, 1H, NH). ^{13}C NMR (100.6 MHz, DMSO-d6): δ = 20.7 (CH_3), 20.7 (CH_3), 20.8 (CH_3), 24.6 (C2), 27.9 ($3CH_3$, *t*Bu), 28.0 ($6CH_3$, *t*Bu), 28.3 (C3), 39.7 (C12), 40.4 (C11), 51.3 (C1), 55.7 (8C, C-cyclen), 56.1 (4C, C14, C17, C20, C23), 63.6 (C9), 69.6 (C7), 72.0 (C5), 74.6 (C6), 76.0 (C8), 76.9 (C4), 82.0 ($6C_{qtBu}$), 82.0 ($3C_{qtBu}$), 156.4 (C═O_{carb}), 169.8 (C═O), 169.8 (C═O), 170.3 (C═O), 172.0 (C═O), 172.3 (3C═O). HRMS (ESI, $C_{46}H_{80}N_9O_{16}$: $[M + H]^+$) calcd 1014.5723, found 1014.5741.

*Compound **11**.* To a suspension of compound **10** (73 mg; 0.072 mmol) in water (1.13 mL) was added HCl 37% (375 μL). The reaction mixture was stirred at room temperature for 4 h and evaporated under reduce pressure using MeOH as co-solvent to afford **11** (51.7 mg). Yield quantitative. Yellow solid. Mp: 93–95 °C; $[\alpha]_D$: −7.8 (c 0.03; EtOH); IR film (ν, cm^{-1}): 3260, 3082, 2932, 2864, 2095, 1722, 1674, 1539, 1385, 1352, 1211, 1084; ^1H NMR (400 MHz, D_2O): δ 1.44–1.57 (m, 1H, H3a), 1.64–1.76 (m, 1H, H2a), 1.76–1.86 (m, 1H, H2a), 1.88–1.98 (m, 1H, H3b), 3.22 (appt, 1H, $J_{5,4} = J_{5,6} = 8.5$ Hz, H5), 3.24–3.60 (m, 25H, H4, H7, H12, H11, H6, H14, 16Hcyclen), 3.37 (t, 2H, $J_{1,2a} = J_{1,2b} = 7.0$ Hz, H1), 3.53–3.61 (m, 1H, H8), 3.73–4.00 (m, 6H, H17, H20, H23), 4.24 (dd, 1H, $J_{9a,9b} = 11.5$ Hz, $J_{9a,8} = 6.5$ Hz, H9a), 4.37 (bd, 1H, H9b). ^{13}C NMR (100.6 MHz, D_2O): δ 24.2 (C2), 27.8 (C3), 39.3 (C12), 39.6 (C11), 44.4–50.4 (8C, C-cyclen), 50.9 (C1), 55.0 (4C, C14, C17, C20, C23), 64.0 (C9), 69.9 (C7), 73.4 (C5), 77.2 (C6), 77.4 (C8), 79.1 (C4), 158.4 (C═O_{carb}), 175.3 (C═O), 175.6 (3C═O). HRMS (ESI, $C_{28}H_{49}N_9O_{13}Na$: $[M + Na]^+$) calcd 742.3348, found 742.3252; (ESI, $C_{28}H_{48}N_9O_{13}Na_2$: $[M - H + 2Na]^+$) calcd 764.3167, found 764.3066.

*Compound **13**.* To a solution of azido derivative **11** (4.3 mg, 0.006 mmol) diluted in 0.6 mL of water, were added at room temperature a solution of c(RGDfK) derivative **12** (4.8 mg, 0.006 mmol) diluted in 1 mL of *tert*-butanol, a solution of sodium ascorbate (0.018 mmol) in 0.2 mL of water and a solution of $Cu(OAc)_2$ (0.009 mmol) in 0.2 mL of water. The solution was stirred 5 h at room temperature, then $Na_2S \cdot 9H_2O$ (8.5 mg, 0.036 mmol) was added. The mixture was stirred 15 min. Black precipitate appeared immediately, the mixture was filtered on a Celite pad, then freeze-dried. Purification was achieved on Sephadex LH20 resin. Elution with water provided pure compound **13** (6 mg). Yield 72%. White foam. ^1H NMR (400 MHz, D_2O): δ 0.72–0.86 (m, 2H, H32), 1.17–1.29 (m, 2H, H31), 1.38–1.51 (m, 2H, H33a, H2a), 1.51–1.58 (m, 2H, H42), 1.58–1.75 (m, 2H, H33b, H3a), 1.78–1.95 (m, 2H, H2b, H41a), 1.94–2.15 (m, 2H, H41b, H3b), 2.56 (dd, 1H, $J_{38a,38b} = 16.5$ Hz, $J_{38a,37} =$

7.0 Hz, H38a), 2.65 (bt, 2H, $J_{29,28}$ = 7.0 Hz, H29), 2.70 (dd, 1H, $J_{38b,37}$ = 7.0 Hz, H38b), 2.93–3.05 (m, 4H, H28, H30), 3.07–3.36 (m, 26H, H5, H39, H43, H4, H12, H11, 16H cyclen), 3.37–3.56 (m, 15H, H1, CH_2Bn, H7, H6, H14, H17, H20, H23), 3.61 (dd, 1H, $J_{9a,9b}$ = 11.5 Hz, $J_{9a,8}$ = 7.5 Hz, H9a), 3.67 (dd, 1H, $J_{9a,8}$ = 4.5 Hz, H9b), 3.80–3.92 (m, 3H, H8, H34), 4.50 (d, 1H, J = 14.0 Hz, CH_2Bn), 4.43 (app t, 1H, J = 7.0 Hz, H40), 4.56–4.63 (m, 1H, H35), 4,67–4.75 (m, 1H, H37), 7.23–7.29 (m, 3H, H_{Ar}), 7.31–7.38 (m, 2H, H_{Ar}), 7.83 (bs, 1H, H26). ^{13}C NMR (100.6 MHz, D_2O): δ 21.2 (C28), 22.4 (C32), 24.2 (C2), 27.3, 27.4, 27.6, 27.6 (C41, C42, C31, C3), 30.0 (C33), 35.3 (C29), 37.8 (2C, C39, C30), 38.9 (3C, C38, C12, C11), 40.5 (C43), 43.8 (C36CH_2Bn), 47.8–48.7 (8C, C-cyclen), 50.0 (2C, C40, C1), 50.8 (C37), 55.2 (C35 or C34), 55.5 (C34 or C35), 58.5–59.0 (4C, C14, C17, C20, C23), 63.2 (C9), 72.0 (C7), 72.1 (C8), 73.4 (C5), 77.2 (C6), 78.8 (C4), 123.3 (C26), 127.2 (C_{Ar}), 128.8 (2C_{Ar}), 129.2 (2C_{Ar}), 136.0 (C_{qAr}), 146.3 (C27), 155.0 (C=N), 157.0 (C=O_{carb}), 171.3 (C=O), 172.5 (C=O), 172.6 (C=O), 173.4 (C=O), 173.6 (C=O), 174.3 (C=O), 174.4 (C=O), 175.8 (C=O), 176.2 (C=O), 177.9 (C=O), 178.0 (C=O). HRMS (ESI, $C_{60}H_{95}N_{18}O_{21}K$: $[M + K]^{2+}$) calcd 721.3275, found 721.3256.

Integrin $\alpha_v\beta_3$ binding assay

The affinity of compounds for integrin protein was evaluated in terms of the half maximal inhibitory concentration (IC_{50} values) through a solid-phase assay as previously described by Tobias G. Kapp and al.[47] Briefly, the surface of Maxisorp microplates (NUNC, Thermoficher scientific, France) was coated with 1 μg mL^{-1} human vitronectin (Bio-techne, France), overnight at +4 °C. The non-specific sites were blocked with TSB buffer (20 mM Tris–HCl, 150 mM NaCl, 1 mM $CaCl_2$, 1 mM $MgCl_2$, 1 mM $MnCl_2$, pH 7,5, 1% BSA) (Sigma-Aldrich, France) for 1 h at 37 °C. Binding of compounds was assessed using 2 μg mL^{-1} integrin $\alpha_v\beta_3$ (Bio-techne, France) in the presence of dilution series of compounds or two reference molecules: c(RGDfK) (Bachem, Germany) and echistatin (Bio-techne, France), as positive control. After 1 h incubation at room temperature, the plates were washed and the amount of bound integrin was stained by incubation with 2 μg mL^{-1} mouse anti-human CD51/61 (BD Pharmingen, France) and 1 μg mL^{-1} anti-mouse IgG horseradish peroxidase conjugate antibody (Bio-techne, France). The enzymatic reaction was allowed in the dark by addition of substrate (Bio-techne, France) and stopped after 10 min by the addition of H_2SO_4 (Stop Solution, Bio-techne, France). The optical densities were measured at 450 nm. Values were blank subtracted and results were expressed as a mean of relative absorbance percentage to wells containing only integrin αvβ3 of triplicate measurements. Affinities were estimated as IC_{50} values (*i.e.* the concentration of compounds that displaced 50% of integrin binding) calculated using one-site fit log-IC_{50} non-linear analysis regression of GraphPad Prism 6 software (v 6.05, USA).

Radiochemistry

The ^{68}Ga-labelling of **13** was performed using a mAIO synthesizer (Trasis, Ans, Belgium) with removable cassettes. The ^{68}Ge/^{68}Ga generator (Galiapharm; Eckert & Ziegler Europe) was eluted with 5 mL of a 0.1 M HCl solution. **13** (50 μg, 34 nmol) previously solubilized in 1 mL of acetate buffer solution (0.7 M), was added to the eluted solution. The mixture was heated at 110 °C during 10 min. The resulting product, **[^{68}Ga]13**, was trapped on a HLB Oasis cartridge. The product was eluted from the cartridge with 0.6 mL of ethanol. The cartridge was rinsed with 5 mL of NaCl 0.9%. **[^{68}Ga]13** was produced with a decay corrected (dc.) radiochemical yield of 78 ± 3% (n = 20).

Animal models and experimental plan

All protocols were approved by the Lorraine Ethics Committee No 68 according to Guidelines of Animal Care and Use (APAFIS#25133-2020041509493813). Tumor xenografts were obtained in mice flanks as described previously.[44] Six-week-old female immunodeficient (nu/nu) NMRI mice (n = 3), weighing 26–27 g, were obtained from Janvier Laboratories (Le Genest Saint Isle, France) and housed in ventilated cages including filter tops with an ad libitum access to food and water. Xenograft tumor was induced in all mice through subcutaneous flank injections of 2 × 10^6 of human U87-MG cells. Tumor growth was assessed twice weekly, according to tumor volume (in mm^3) calculated with the formula $d2 \times D/2$, where d and D represent the shortest and longest diameters, respectively, calculated in millimeter with a caliper (+decrescent PRC, EDVC, France). The average tumor volume was 107 ± 0.4 mm^3.

Small animal PET studies

Mice were anesthetized with 1.5% isoflurane, 10 ± 1 MBq of **[^{68}Ga]13** were injected as a bolus *via* a lateral tail vein. List-mode acquisitions of 120 min durations were initiated a few seconds prior to tracer injection, and the acquired PET data were subsequently reconstructed in 27 consecutive frames (*i.e.*, 5 frames of 120 s duration followed by 22 frames of 5 min duration) using the ordered-subsets expectation maximization 3D algorithm (OSEM3D, 4 iterations, 16 subsets, zoom 1) together with scatter and attenuation corrections based on transmission source measurement. The final voxel size was 0.8 × 0.8 × 0.9 mm^3. Images were visualized as maximum intensity projections and from different slices (sagittal, transverse, coronal) to allow visual and quantitative analysis, for each animal and for each PET tracer. Tumor and various organ activities were determined through SUV mean values within 3D regions of interests (ROI), which were drawn with a dedicated software (Inveon Research Workplace 4.1, Siemens®, Knoxville, USA) on the fusion images encompassing the entire 120 min recording period. Spheroid ROIs were placed inside the tumor, non-target area, brain, heart, liver and kidneys regions with the ROI limits approximating the organ limits as close as possible. Tumor ROIs was obtained with isocontour ROIs and threshold limits of 50%, of the maximal voxel value. All data are expressed as mean ± SD. Unpaired comparison of quantitative variable were performed with Student's t test. P values less than 0.05 were considered as statistically significant.

Author contributions

FlM with the participation of SLL and NPM synthesized all the non-radioactive compounds (**1** to **13**) and completed the NMR

analysis of these compounds. KS synthesized **(Ga)13**, completed the mass spectra analysis and co-wrote the manuscript. VJH with the participation of CB performed *in vitro* integrin binding assay and they co-wrote the manuscript. CC with the participation of SLL and NPM performed the radionuclide-labelling of **13** and wrote radiochemistry section. FM and CB co-wrote the ethical request for project authorization. JP and CB provided the animal models. ER with the collaboration of JP and FM performed the experimental studies in mice. FM performed images analysis on the small animal PET. FM and PYM co-wrote the manuscript. SLL and NPM designed the study and wrote the manuscript. All authors read and approved the final manuscript.

Conflicts of interest

There are no conflicts to declare.

Acknowledgements

This work was supported by NancycloTEP. We thank F. Dupire and S. Adach for technical assistance. We gratefully acknowledge the financial support of the "Contrat de Plan Etat-Région" (CPER) from French government and Grand Est Regional Council.

References

1 J. A. Jackson, I. N. Hungnes, M. T. Ma and C. Rivas, *Bioconjugate Chem.*, 2020, **31**, 483–491.
2 J. Rafferty, H. Nagaraj, A. P. McCloskey, R. Huwaitat, S. Porter, A. Albadr and G. Laverty, *Curr. Med. Chem.*, 2016, **23**, 4231–4259.
3 A. L. Tornesello, M. L. Tornesello and F. M. Buonaguro, *Mini-Rev. Med. Chem.*, 2017, **17**, 758–770.
4 T. Vucko, N. Pétry, F. Dehez, A. Lambert, A. Monari, C. Lakomy, P. Lacolley, V. Regnault, C. Collet, G. Karcher, N. Pellegrini-Moïse and S. Lamandé-Langle, *Bioorg. Med. Chem.*, 2019, **27**, 4101–4109.
5 C. Collet, T. Vucko, J. Ariztia, G. Karcher, N. Pellegrini-Moïse and S. Lamandé-Langle, *React. Chem. Eng.*, 2019, **4**, 2088–2098.
6 C. L. Charron, A. L. Farnsworth, P. D. Roselt, R. J. Hicks and C. A. Hutton, *Tetrahedron Lett.*, 2016, **57**, 4119–4127.
7 H. Chen, G. Niu, H. Wu and X. Chen, *Theranostics*, 2016, **6**, 78–92.
8 E. Giovannini, G. Giovacchini, E. Borso, P. Lazzeri, M. Riondato, R. Leoncini, V. Duce and A. Ciarmiello, *Curr. Radiopharm.*, 2019, **12**, 11–22.
9 O. Morris, M. Fairclough, J. Grigg, C. Prenant and A. McMahon, *J. Labelled Compd. Radiopharm.*, 2019, **62**, 4–23.
10 A. L. Tornesello, L. Buonaguro, M. L. Tornesello and F. M. Buonaguro, *Molecules*, 2017, **22**, 1282–1291.
11 S. Richter, M. Wuest, C. Bergman, J. Way, S. Krieger, B. E. Rogers and F. Wuest, *Bioconjugate Chem.*, 2015, **26**, 201–212.
12 R. Haubner, B. Kuhnast, C. Mang, W. A. Weber, H. Kessler, H. J. Wester and M. Schwaiger, *Bioconjugate Chem.*, 2004, **15**, 61–69.
13 K. Stromgaard and T. Hoeg-Jensen, in *Pharmaceutical Formulation Development of Peptides and Proteins – Peptide and protein derivatives*, ed. L. Hovgaard, S. Frokjaer and M. Van de Weert, Taylor & Francis Boca Raton, 2nd edn, 2013, pp. 131–148.
14 M. Alipour, M. Baneshi, S. Hosseinkhani, R. Mahmoudi, A. J. Arabzadeh, M. Akrami, J. Mehrzad and H. Bardania, *J. Biomed. Mater. Res., Part A*, 2020, **108**, 839–850.
15 S. Asati, V. Pandey and V. Soni, *Int. J. Pept. Res. Ther.*, 2019, **25**, 49–65.
16 C. Collet, F. Maskali, A. Clément, F. Chrétien, S. Poussier, G. Karcher, P.-Y. Marie, Y. Chapleur and S. Lamandé-Langle, *J. Labelled Compd. Radiopharm.*, 2016, **59**, 54–62.
17 Y. Chapleur, S. Lamandé, C. Collet and F. Chrétien, PCT Int., WO 2014006022 A1 20140109, 2014.
18 N. Alexander, R. Vali, H. Ahmadzadehfar, A. Shammas and S. Baruchel, *Curr. Radiopharm.*, 2018, **11**, 14–21.
19 S. Narayana, M. Chilla, C. Henoumont, L. Vander Elst, R. N. Muller and S. Laurent, *Magn. Reson. Imaging*, 2017, **57**, 800–808.
20 K. Tanaka and K. Fukase, *Org. Biomol. Chem.*, 2008, **6**, 815–828.
21 M. Guleria, T. Das, J. Amirdhanayagam, H. D. Sarma and A. Dash, *Nucl. Med. Biol.*, 2019, **78–79**, 31–40.
22 R. Viswas, E. Alizadeh, W. Bernhard, S. V. Hartimath, W. Hill, R. Chekol, K. M. Barreto, C. R. Geyer and H. Fonge, *Mol. Pharm.*, 2019, **16**, 4807–4816.
23 G. Giannini, F. M. Milazzo, G. Battistuzzi, A. Rosi, A. M. Anastasi, F. Petronzelli, C. Albertoni, L. Tei, L. Leone, L. Salvini and R. De Santis, *Bioorg. Med. Chem.*, 2019, **27**, 3248–3253.
24 J. W. M. Bulte, in *The Chemistry of Contrast Agents in Medical Magnetic Resonance Imaging*, ed. A. E. Merbach and E. Toth, Wiley, Chichester, 2001.
25 S. Jenni, F. Bolze, C. S. Bonnet, A. Pallier, A. Sour, E. Tóth, B. Ventura and V. Heitz, *Inorg. Chem.*, 2020, **59**, 14389–14398.
26 J. R. Dilworth and S. I. Pascu, in *The radiopharmaceutical chemistry of gallium(III) and indium(III) for SPECT imaging*. ed. N. Long and W.-T. Wong, From Chemistry of Molecular Imaging, 2015, pp. 165–178.
27 G. J. Stasiuk and N. J. Long, *Chem. Commun.*, 2013, **49**, 2732.
28 N. Viola-Villegas and R. P. Doyle, *Coord. Chem. Rev.*, 2009, **253**, 1906–1925.
29 P. Antunes, M. Ginj, M. A. Walter, J. Chen, J.-C. Reubi and H. R. Maecke, *Bioconjugate Chem.*, 2007, **18**, 84–92.
30 O. Kazuma, J. Yu, A. Ishizaki, M. Yokokawa, M. Kitamura, Y. Kitamura, K. Shiba and A. Odani, *Bioconjugate Chem.*, 2015, **26**, 1561–1570.
31 I. Dijkgraaf, C.-B. Yim, G. M. Franssen, R. C. Schuit, G. Luurtsema, S. Liu, W. J. G. Oyen and O. C. Boerman, *Eur. J. Nucl. Med. Mol. Imaging*, 2011, **38**, 128–137.
32 A. Barge, L. Tei, D. Upadhyaya, F. Fedeli, L. Beltrami, R. Stefanìa, S. Aime and G. Cravotto, *Org. Biomol. Chem.*, 2008, **6**, 1176–1184.

33 E. Leclerc, X. Pannecoucke, M. Etheve-Quelquejeuc and M. Sollogoub, *Chem. Soc. Rev.*, 2013, **42**, 4270–4283.
34 S. Passemarda, D. Staedlera, L. Ucnováa, G. S. Schneitera, P. Konga, L. Bonacinab, L. Juillerat-Jeanneretc and S. Gerber-Lemaire, *Bioorg. Med. Chem. Lett.*, 2013, **23**, 5006–5010.
35 A. Y. Lebedev, J. P. Holland and J. S. Lewis, *Chem. Commun.*, 2010, **46**, 1706–1708.
36 O. Schnell, B. Krebs, E. Wagner, A. Romagna, A. J. Beer, S. J. Grau, N. Thon, C. Goetz, H. A. Kretzschmar, J. C. Tonn and R. H. Goldbrunner, *Brain Pathol.*, 2008, **18**, 378–386.
37 J. D. Hood and D. A. Cheresh, *Nat. Rev. Cancer*, 2002, **2**, 91–100.
38 D. E. Levy, *Strategies towards C-glycosides in The Organic Chemistry of Sugars*, ed. D. E. Levy and P. Fügedi, CRC Press, 2006, pp. 269–348.
39 C. Decristoforo, I. Hernandez Gonzalez, J. Carlsen, M. Rupprich, M. Huisman, I. Virgolini, H.-J. Wester and R. Haubner, *Eur. J. Nucl. Med. Mol. Imaging*, 2008, **35**, 1507–1515.
40 Z. Novy, J. Stepankova, M. Hola, D. Flasarova, M. Popper and M. Petrik, *Molecules*, 2019, **24**, 2496.
41 M. I. Tsionou, C. E. Knapp, C. A. Foley, C. R. Munteanu, A. Cakebread, C. Imberti, T. R. Eykyn, J. D. Young, B. M. Paterson, P. J. Blower and M. T. Ma, *RSC Adv.*, 2017, **7**, 49586–49599.
42 E. W. Price and C. Orvigt, *Chem. Soc. Rev.*, 2014, **43**, 260.
43 W. Chen, *J. Nucl. Med.*, 2007, **48**, 1468–1481.
44 Z. B. Li, K. Chen and X. Chen, *Eur. J. Nucl. Med. Mol. Imaging*, 2008, **35**, 1100–1108.
45 P. A. Knetsch, M. Petrik, C. M. Griessinger, C. Rangger, M. Fani, C. Kesenheimer, E. von Guggenberg, B. J. Pichler, I. Virgolini, C. Decristoforo and R. Haubner, *Eur. J. Nucl. Med. Mol. Imaging*, 2011, **38**, 1303–1312.
46 S. Isal, J. Pierson, L. Imbert, A. Clement, C. Collet, S. Pinel, N. Veran, A. Reinhard, S. Poussier, G. Gauchotte, S. Frezier, G. Karcher, P.-Y. Marie and F. Maskali, *EJNMMI Res.*, 2018, **8**, 51.
47 T. G. Kapp, F. Rechenmacher, S. Neubauer, O. V. Maltsev, E. A. Cavalcanti-Adam, R. Zarka, U. Reuning, J. Notni, H. J. Wester, C. Mas-Moruno, J. Spatz, B. Geiger and H. Kessler, *Sci. Rep.*, 2017, **7**, 39805–39821.